RSC Sustainability

ROYAL SOCIETY OF CHEMISTRY

PAPER

View Article Online
View Journal | View Issue

Cite this: *RSC Sustainability*, 2024, **2**, 223

Nitrogen-doped carbon quantum dots from biomass as a FRET-based sensing platform for the selective detection of H_2O_2 and aspartic acid†

K. Sandeep Raju, Gouri Sankar Das and Kumud Malika Tripathi *

Received 25th September 2023
Accepted 10th November 2023

DOI: 10.1039/d3su00343d

rsc.li/rscsus

Hydrogen peroxide (H_2O_2) with strong oxidizing properties and a volatile nature has a potential role in biological systems and industrial applications. Developing an optical "on–off–on" probe for the efficient detection of H_2O_2 is crucial for health, environmental safety, and diagnostic applications. Herein, sustainable N-doped carbon quantum dots (N-CQDs) were explored as optical probes for the selective discrimination of H_2O_2 and aspartic acid in aqueous media based on simple photoluminescence "turn on" and "turn off" mechanisms. N-CQDs were synthesized from *Moringa oleifera* (drumstick leaves) used as both a carbon and nitrogen source. The synergistic effect of N-doping, oxygenous surface functional groups and structural advantages lead to high selectivity and good sensing performance with a LOD value of 26.4 mM and 134.2 nM for H_2O_2 and aspartic acid, respectively. The simple synthesis process and structural advantage of N-CQDs showed the potential for the detection of reactive oxygen species and biomolecules with high sensitivity and selectivity in an aqueous medium for diagnostic applications and human health monitoring.

Sustainability spotlight

The development of environmentally friendly technology for precise detection of biomarkers is essential at a time when environmental sustainability and human health are of the highest priority. Our research focuses on nature's resources to build an optical "on–off–on" probe with important diagnostic and environmental applications. In this approach, N-CQDs were synthesized by using an environmentally friendly process from natural resources *Moringa oliefera* (drumstick leaves). N-CQDs have a unique photoluminescent property, which is beneficial for the detection of biomarkers and biomolecules by adapting the "PL turn on" and "PL turn off" mechanism attributed to the presence of oxygen and nitrogenous functional groups. It is essential to detect H_2O_2 for the early diagnosis of stress-related diseases accurately without using any sophisticated and costly methods (SDG 3). The use of drumstick leaves as a carbon source for N-CQD synthesis is an example of a sustainable and responsible approach (SDG 12) (SDG 15). This study is an example of collaborating with scientists, environmentalists, healthcare professionals, various field experts, and interdisciplinary researchers by utilizing N-CQDs to solve various challenges (SDG 17) together to solve complex problems. The development of an optical probe for sensing H_2O_2 and aspartic acid is not only a solution for health and environmental monitoring but also satisfies multiple Sustainable Development Goals SDG 3, SDG 12, SDG 15, SDG 17 in creating a healthier and more sustainable future for everyone.

1. Introduction

Changes in lifestyle and personalized medical devices has increased demands for low-cost biosensors for the real-time identification and continuous monitoring of biomarkers.[1] Recognition of particular biomarkers is spurred by unprecedented interest in the early-stage diagnosis of diseases, human health monitoring, and food safety.[2,3] Because of emerging diseases and pandemics, the healthcare system has experienced a heightened value of technologies.[1] Several new healthcare programmes and next-generation biomedical technologies require handy and miniaturized point-of-care devices.[4,5] The detection of biomarkers has been proven as a valid alternative for the detection of cancer and other infectious diseases. Different biomarkers, because of alterations in metabolism, are present in body fluids and exhaled breath, and exhibit potential opportunities for disease diagnosis.[6,7] The accurate identification and determination of these biomarkers can reveal the states and stages of a particular disease or individual. Thus, rapid and real time detection of biomarkers is crucial in biomedical diagnosis.[3]

Hydrogen peroxide (H_2O_2) is a well-recognized reactive oxygen species (ROS), which is associated with cell damage and many other biological activities in living beings.[8] H_2O_2 is a short-lived by-product of several metabolic processes, such as cholesterol oxidase, glucose oxidase, choline oxidase, and so on.[9,10] The availability of H_2O_2 in the human body induces

Department of Chemistry, Indian Institute of Petroleum and Energy, Visakhapatnam, Andhra Pradesh, 530003, India. E-mail: kumud20010@gmail.com; kumud@iipe.ac.in

† Electronic supplementary information (ESI) available. See DOI: https://doi.org/10.1039/d3su00343d

various oxidative stresses, such as high active oxidation of deoxyribonucleic acid (DNA), proteins, ribonucleic acid (RNA), and membrane lipids.[11,12] However, several studies have suggested that H_2O_2 plays a vital role in pathological and physiological processes as an emerging biomarker for the detection of various human diseases and diagnosis of pathological conditions.[13] The various intercellular concentrations of H_2O_2 are more effective for biological functions, and detecting H_2O_2 concentration is challenging. Accurate detection of H_2O_2 concentration is crucial for identifying and monitoring diseases, including tumour growth, Alzheimer's disease, cancer, neurological disorders, and other oxidative stress-related diseases.[8,14,15] Thus, the development of an efficient analytical technique for the accurate and low-cost determination of H_2O_2 is indispensable to conduct clinical diagnoses.

Aspartic acid is a major excitatory neurotransmitter with wide applications in food, medicine and chemicals. Aspartic acid has two isomeric forms, D and L; only the L form shows bioactive properties and may function as a neurotransmitter. L-aspartic acid is an essential proteinogenic amino acid that generates another new amino acid in living organisms.[16–18] Several studies have concluded that a particular level of aspartic acid could not show harmful effects on the human body.[19] However excessive or insufficient amounts of aspartic acid may cause various diseases such as stroke, epilepsy, mental imbalance, chronic fatigue syndrome, and other severe conditions.[20] Aspartic acid content is a crucial potential indicator for the monitoring of physical health.[21,22] Therefore the detection and quantification of L-aspartic acid with high selectivity and sensitivity provides a strategy to diagnose and monitor some diseases in the early stages.

A number of nano-and micro-technology based biosensors have been developed as diagnostic platforms to detect biomarkers.[2] The integration of nanotechnology in biomolecular sensing exhibits potential advantages in contrast to traditional techniques such as low-detection limits, label free detection, real time and quick analysis, and significantly decreased sample sizes.[23] The unique structural characteristics of nanomaterials with high recognition ability of biomolecules offer advanced tools for bioanalysis and further development of biosensors.[24] Nanomaterials-based optical sensors technology offers considerable potential for the detection and discrimination of various low-molecular weight biomolecules because of their excellent selectivity, high sensitivity, quick response, mobile capabilities and simple operational processes.[25] Nanomaterial-based biosensors are emerging as the fastest growing segment in the healthcare industry.[5] In particular, a number of fluorescent nanomaterials, such as colloidal nanoparticles, metal oxides, noble metal nanoparticles, dye-doped materials, metal organic frameworks (MOF) and nano carbons have been investigated as optical sensors for the selective detection of biomolecules.[23,26] Nanomaterials with good optical properties and optical stability are quite successful in biomedical sensing applications. However, most of the nanomaterials except nano-carbons suffer photodecomposition and photo blinking with potential hazards and high costs.[27,28] While nano-carbons do not suffer from low photo stability, they do exhibit limitations such as low quantum yield, complex synthesis protocols, and associated environmental concerns and toxicity. In light of these challenges, green synthesized nano-carbons with better biocompatibility and photo-stability are currently being explored in the domain of optical sensors to achieve desirable biomolecular sensing technology.

Carbon quantum dots (CQDs) represent a novel class of nanostructured carbon-based zero-dimensional (0D) fluorescent materials used in bio-sensing applications supporting high aqueous solubility, biocompatibility, tunable fluorescence emission, low toxicity, photo response, high photostability, and excellent optoelectronic properties.[29,30] CQDs are π-conjugated spherical nanostructures having size less than 10 nm with quantum confinement and crystalline structure.[23] CQDs have been used in a number of diagnostic, biosensing and biological imaging applications.[24,31] The tunable emissions of CQDs with unique characteristic emissions over a broad spectrum and narrow absorption exhibit significant potential for the fabrication of fluorescence resonance energy transfer (FRET) or quenching mechanism based biosensors.[24] In addition, ease of functionalization, high aqueous solubility and size-controlled synthesis from a variety of green precursors combine to make CQDs one of the research hotspots in FRET-based biosensors.[32]

Biomass is widely accepted as a natural alternative of expensive and chemical based precursors for the green synthesis of CQDs. In addition, the transformation of biomass into CQDs realizes the reasonable disposal of solid waste into value added products for sustainable development.[33,34] Various techniques have been used for the synthesis of CQDs such as microwave-assisted carbonization, electrochemical, pyrolysis, ultrasound, and hydrothermal synthesis.[35–38] The hydrothermal method is one of the efficient thermochemical processes for the synthesis of CQDs from biomass because of its simplicity, cost-effectiveness, and one-step synthesis protocol.[39] Furthermore the fluorescence emission and quantum yield of CQDs can be easily tailored by appropriate heteroatom doping. Incorporation of heteroatoms such as boron, nitrogen, silicon, phosphorus, and sulphur can significantly enhance the optical properties and quantum yield.[40] Among all the heteroatoms, nitrogen can efficiently interact with carbon atoms to form a strong covalent bond and fit well into the lattice position in CQDs. The carbon and nitrogen atoms have similar atomic sizes and appear nearest to each other in the periodic table.[41] Nitrogen-doped CQDs (N-CQDs) produce energy states that can absorb excited electrons and increase the electron density and fluorescence properties.[42]

Herein, N-CQDs were synthesized by a facile, one-step and green process using drumstick leaves as a precursor for both carbon and nitrogen. The as-synthesized CQDs without any further surface passivation or composite fabrication were explored as a FRET based sensor for the discrimination of H_2O_2 and aspartic acid with high sensitivity and selectivity. The intensity of the fluorescence emissions of CQDs was efficiently quenched by the successive addition of H_2O_2. The calculated detection limit for H_2O_2 was 26.4 mM. The restoration in quenched fluorescence intensity of CQDs was observed by the selective accumulation of aspartic acid with a LOD of 134.2 nM.

The N-CQDs have been successfully used as an "on–off–on" fluorescence probe for the selective determination of H_2O_2 and aspartic acid, suggesting its practical application in biomedical diagnosis.

2. Experimental section

2.1 Materials

Laboratory-grade chemicals were used in all the experiments without any further treatment. H_2O_2 and other biomolecules such as L-aspartic acid, L-valine, citric acid, oxalic acid, tryptophan, dextrose, sucrose, glucose, malic acid, methionine, maltose, glutamic acid, arabinose, and xylose were purchased from Merck India. DI water was used to prepare all aqueous solutions until stated.

2.2 Synthesis of N-CQDs

N-CQDs were synthesized through a very simple, one-step process using *Moringa oleifera* (drumstick leaves) as a carbon and nitrogen source. Drumstick leaves were collected and washed with distilled water for the removal of dust. The drumstick leaves were crushed using a kitchen mixture grinder and transferred into a hydrothermal autoclave reactor. Afterwards the hydrothermal reactor was heated at 180 °C for 24 h. After 24 hours of heating, the hydrothermal reactor was allowed to cool down naturally at ambient conditions. The final solution was collected through filtration using 0.22 μm filter paper and used as is without any further treatment. For reproducibility, drumstick leaves were collected from at least six diverse states of India.

2.3 Procedure for spectrophotometric determination of H_2O_2 and aspartic acid

The fluorescence-based sensing behaviour of N-CQDs were investigated in the presence of common reactive species (reactive oxygen species) H_2O_2 and L-aspartic acid at room temperature in an aqueous solution. For selectivity, 125 μL of N-CQDs were added to 100 mL of water, initially selectivity was performed between H_2O_2 and water. A 5 μL of different concentrations of H_2O_2 were added into 2 mL of an aqueous solution of N-CQDs, and PL spectra were monitored at a 380 nm excitation wavelength and an inlet and outlet slit of 1.5 nm after 5 min incubation. The PL intensity of the as-synthesized N-CQDs was "turned off" by adding H_2O_2 to the system.

Sensing of L-aspartic acid was done by interaction of various biomolecules such as L-aspartic acid, L-valine, citric acid, oxalic acid, tryptophan, dextrose, sucrose, glucose, malic acid, methionine, maltose, glutamic acid, arabinose, and xylose in 10 mL solution with H_2O_2/N-CQDs solution; among all the biomolecules L-aspartic acid shows the maximum PL regain. A 10 μM aqueous L-aspartic acid solution was added to the N-CQDs/H_2O_2 system in aliquots.

2.4 Instrumentation

Transmission electron microscopy (TEM) and high-resolution TEM (HRTEM) images were taken using a Tecnai G2 at an operating voltage of 200 kV. Samples were prepared by drop casting of N-CQDs over the surface of a carbon coated copper grid and drying in a vacuum oven at 30 °C for 15 h. The Fourier transform infrared (FT-IR) spectrum was obtained by using a Bruker Alpha II, FT-IR spectrometer. UV absorption spectra were recorded using a LABINDIA UV 3200 UV/VIS spectrophotometer. An ESCA$^+$ Omicron Nanotechnology (Oxford Instruments) instrument was used for the XPS analysis with an Al K_α X-ray source. Fluorescence spectra of N-CQDs were obtained by using Horiba fluoromax-4 with an inlet and exit slit of 1.5 nm.

3. Results and discussions

The surface rich N-CQDs were synthesized using a one-step and facile hydrothermal process. Fig. 1 describes the synthesis procedure of N-CQDs, in which *moringa oleifera* (drumstick leaves) are used both as a carbon and as a nitrogen precursor. The formation of N-CQDs involves a series of reactions such as fragmentations of molecules, dehydration, pyrolysis, polymerization to carbon clusters and aromatization followed by surface functionalization through carbonization.[33] The N-CQDs were collected by filtration with 0.22 μm filter paper. As-synthesized N-CQDs without any further treatment such as surface passivation/composite fabrication or integration of a photoreceptor was used for the development of an "on–off–on" probe for the detection of H_2O_2 by fluorescence quenching and L-aspartic acid by fluorescence recovering, as shown in Fig. 1.

3.1 Characterization of N-CQDs

The size, shape, and morphology of the as-synthesized N-CQDs were examined through high-resolution transmission electron micrographic (HR-TEM) measurements. The TEM images of N-CQDs in Fig. 2a–c show a monodisperse and spherical shape. The N-CQD appeared with a limited distribution of size, which was evaluated from the statistical calculation as shown in Fig. 2d, which indicates that the as-synthesized N-CQDs have an average diameter of 2–3 nm. The HR-TEM images of N-CQDs show the crystal structure (inside the sphere) and the amorphous structure (surface of the sphere) in Fig. 2e and f. The lattice distance of 0.28 nm (Fig. 2f, as shown by white lines), which is near to the regular graphite (100) plane confirms the crystalline nature of N-CQDs.[43]

The FT-IR spectral analysis was utilized to characterize the surface oxygenated and nitrogenous functional groups on N-CQDs, as shown in Fig. 3a. The vibrations for N–H and O–H stretching appear at ~3000–3500 cm^{-1}.[44] The characteristic doublet for C–H vibration is observed at ~2927 and ~2858 cm^{-1}.[45] The intense peak at 1627 cm^{-1} attributed to the combined vibrations of C=N and C=O bonds. The C–N, C=C, and C–O bonds show stretching vibrations peaks at ~1398 cm^{-1}, ~1302 cm^{-1}, and ~1098 cm^{-1}, respectively.[46,47] The peak for the bending mode of C–H bond vibrations occurred at ~706 cm^{-1}.[48] These results suggested that the as-synthesized N-CQDs are highly hydrophilic and have a good dispersibility in aqueous solutions because of the presence of oxygenated and nitrogenous functional groups.

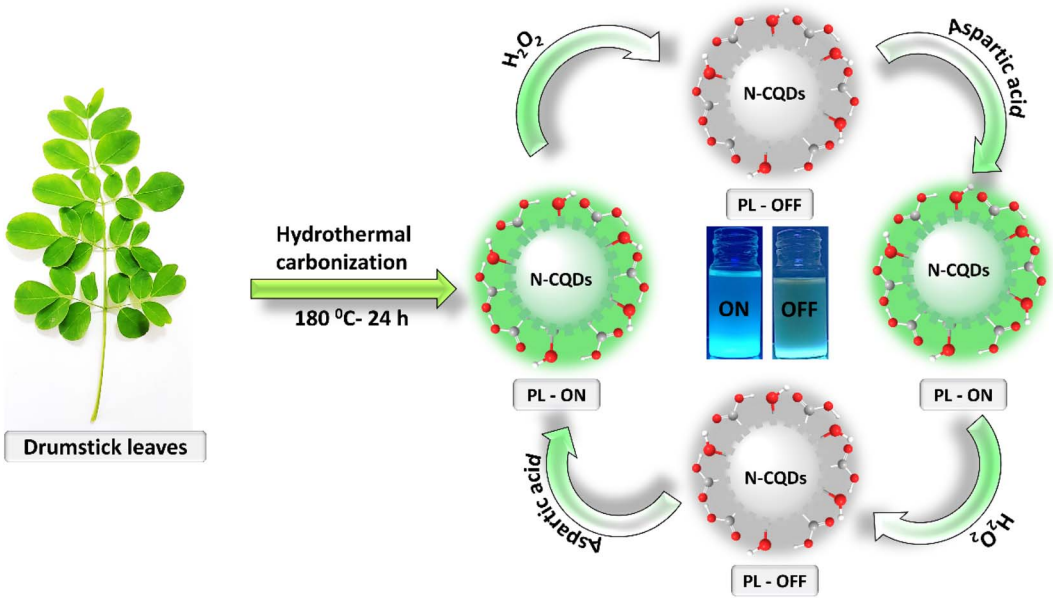

Fig. 1 Schematic representation of synthesis and application of N-CQDs.

XPS measurements were conducted to confirm the nitrogen doping, bonding environment and elemental composition of the N-CQDs. The wide scan XPS spectrum of N-CQDs in Fig. 3b indicates the presence of three peaks at 285.1, 400.0, and 532.1 eV corresponding to carbon, nitrogen, and oxygen elements, with 70.26%, 8.36%, and 21.38% atomic percentages, respectively. The deconvolution of C 1s, N 1s, and O 1s provides the appropriate information of the chemical bonding environment of the elements. The high-resolution C 1s spectrum in Fig. 3c was deconvoluted into five peaks at 284.28 eV (C=C), 286.27 eV (C–O), 285.3 eV (C–N, C–C), 287.58 eV (C=O), and 288.53 eV (COO^-).[48,49] Fig. 3d shows the high-resolution N 1s spectrum, which was further split into three different peaks at 399.18 eV for pyridinic nitrogen, 400.08 eV for pyrrolic nitrogen

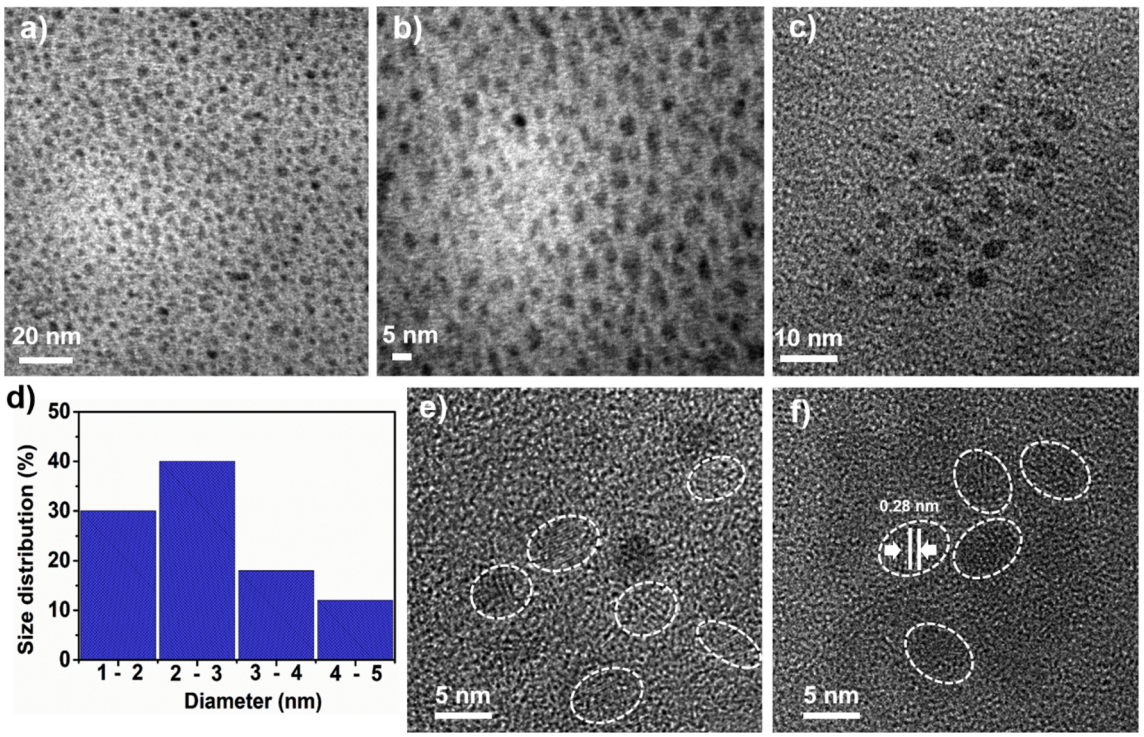

Fig. 2 Structural characterization of N-CQDs. (a–c) TEM images, (d) size distribution histogram of N-CQDs, (e) and (f) HR-TEM images.

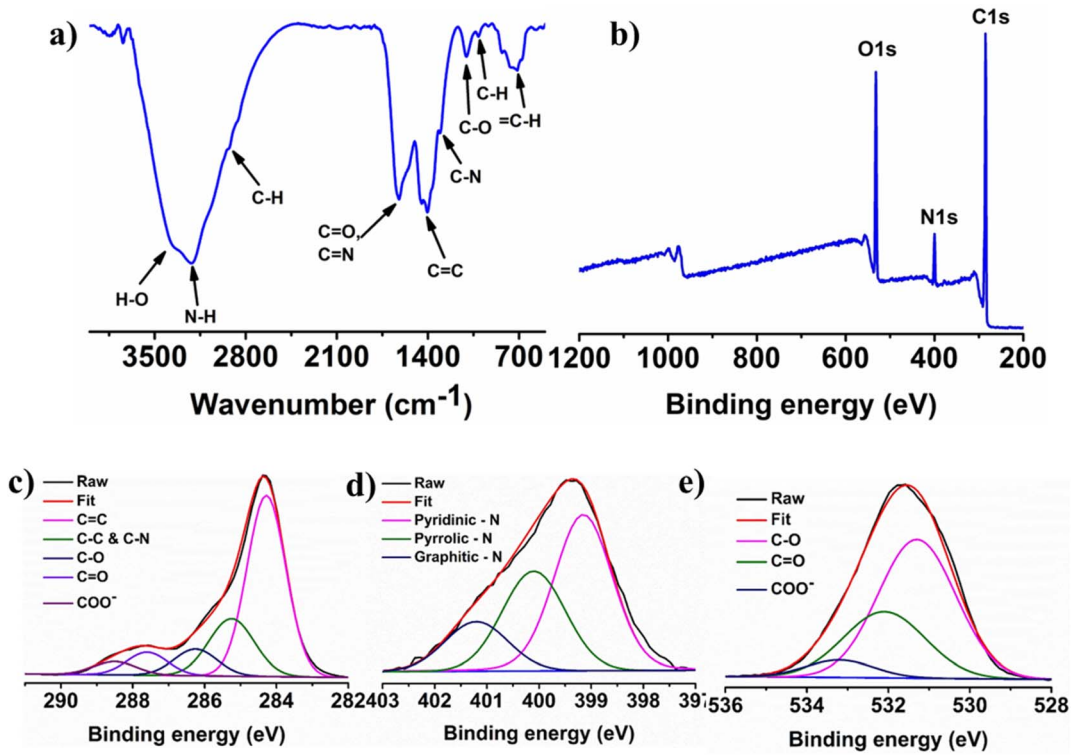

Fig. 3 Structural characterization of N-CQDs. (a) Characterization of functional groups by FTIR spectrum; (b) XPS survey scan; high-resolution spectra of C 1s (c), N 1s (d), and O 1s (e).

and 401.18 eV for graphitic nitrogen. The deconvoluted O 1s spectrum in Fig. 3e shows the three well-defined peaks centered at 531.28, 532.08, and 533.28 eV which are attributed to the C–O, C═O, and COO^- bonding, respectively.[50] The XPS spectra confirmed the different types of chemical bonding of nitrogen atoms with carbons suggesting that nitrogen atoms were successfully incorporated into the graphitic framework of the CQDs. These XPS examination results concurred with the FT-IR results.

3.2 Optical properties

UV-vis absorption and fluorescence spectroscopic analysis were performed for the investigation of the N-CQDs optical properties. The aqueous solution of N-CQDs showed two absorption peaks at ~255 and ~272 nm in the UV-vis absorption spectrum (Fig. 4a). The absorption peak at ~255 nm occurs because of the π–π^* electronic transition from the domains of sp^2 carbons. The absorption band at ~272 nm corresponds to the electronic transition of n-π^* attributed to the non-bonding electrons of the –C═N– and –C═O functional groups of N-CQDs.[51] The digital images of N-CQDs solution in water under the irradiation of different lights are shown in the inset of Fig. 4a. N-CQDs show a pale-yellow colour under visible light (Fig. 4a(I)) and a greenish blue colour was observed under the 365 nm excitation of UV light, as shown in Fig. 4a(II). The PL emissions of N-CQDs at variable excitation wavelengths (280–640 nm) in 20 nm increments is shown in Fig. 4b. The PL spectra indicates that excitation at 360 nm results in maximum emission at 440 nm. In detail, the PL intensity of N-CQDs changes with excitations. The PL intensity gradually increased with the change of excitation from 280 to 360 nm and steadily decreased afterwards from 380 to 640 nm excitation wavelengths. These properties can be described as being due to the electronegativity of heteroatoms, quantum confinement effects, and presence of different surface traps on CQDs.[45,48] The availability of different emissive sites with various nitrogenous and oxygenated functional groups on N-CQDs is responsible for the excitation dependent emissions, which is a characteristic property of CQDs.[52] Fig. 4c shows the back-excitation spectrum of maximum peak value of 367 nm. The PL quantum yield of the as-synthesized N-CQDs is 12.5%. The PL stability of N-CQDs plays a crucial role in potential applications. Fig. 4d shows the emissions of the as-synthesized N-CQDs as synthesized and after three months of storage. The relatively similar PL intensity indicates the high PL stability of N-CQDs solution even after prolonged storage.

3.3 Sensing of H_2O_2 and L-aspartic acid

The sensitive and selective detection of H_2O_2 was explored by utilizing FRET based techniques. The PL emission of as synthesized N-CQDs was turned off (quenched) by the addition of H_2O_2, as shown in Fig. 5a. The smooth and gradual drop in PL emission of N-CQDs by the stepwise addition of H_2O_2 (0–0.4 M) was attributed to the interaction between N-CQDs and H_2O_2. The PL quenching efficiency of N-CQDs shows a linear correlation with an R^2 value of 0.98715 as shown in Fig. 5b. The limit

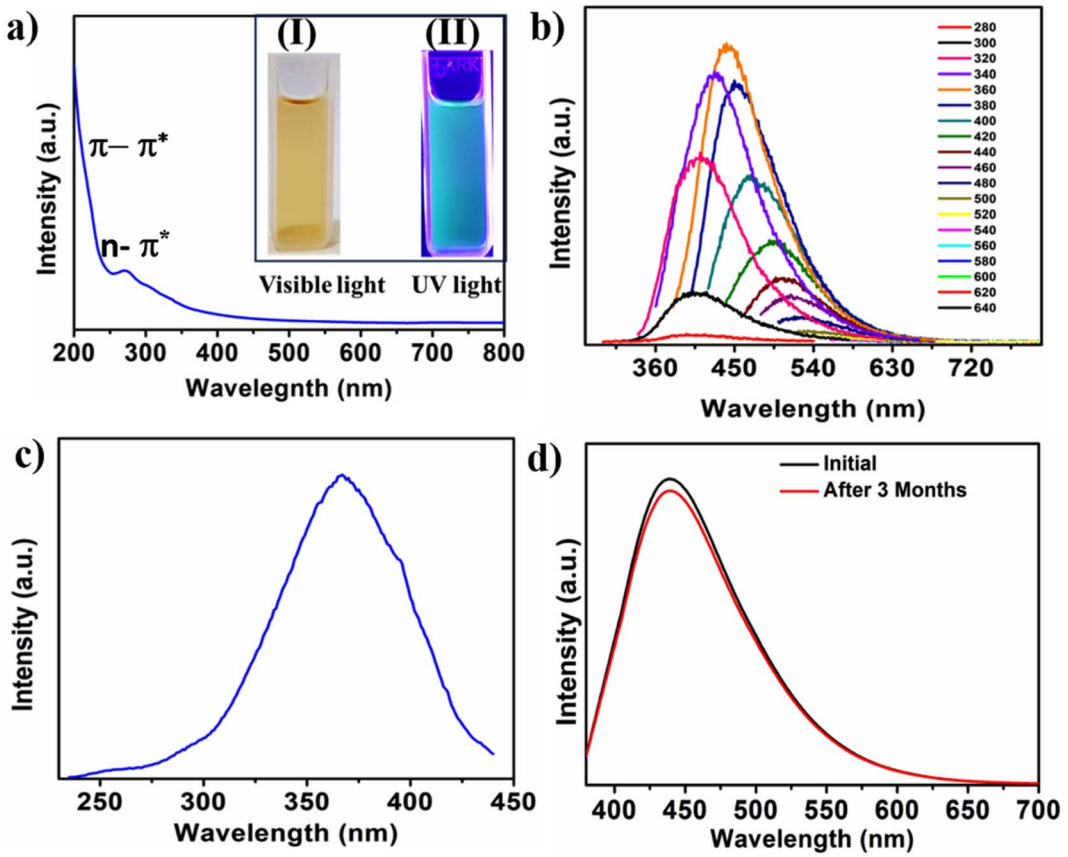

Fig. 4 Optical characterization of N-CQDs. (a) UV-vis spectrum; digital images of N-CQDs in visible light (I) and UV light (II) showing pale yellow and greenish blue colours respectively; (b) PL spectra; (c) back excitation spectrum; (d) PL intensities of N-CQDs initially and after three months of storage.

of detection (LOD) for H_2O_2 was evaluated using the equation LOD = $3\sigma/m$ (where σ and m are the standard deviations and slope of the linear calibration curve).[53] The calculated value of the LOD is 26.4 mM for H_2O_2 in a neutral aqueous solution. A comparative analysis of the LOD of N-CQDs for H_2O_2 is shown in Table S1.† In a comparative study of N-CQDs, the PL quenching effect of H_2O_2 and H_2O was shown in inset of Fig. 5a. The PL intensity was decreased in presence of H_2O because of the dilution effect.

Furthermore, the selective sensing of biomolecules was also evaluated by the addition of an aqueous solution of an analyte to the quenched system of the N-CQDs/H_2O_2. The PL intensity was selectively restored ("turned on") by the addition of L-aspartic acid. Fig. 5c shows the highly selective sensing of L-aspartic acid compared to various interferences such as oxalic acid, L-valine, malic acid, arabinose, dextrose, citric acid, sucrose, tryptophan, glucose, glutamic acid, maltose, rhamnose, maltose, methionine, and xylose. These results suggested that the L-aspartic acid has a high tendency to bind with H_2O_2 and makes N-CQDs accessible. As a result, the PL intensity was restored. The PL emission intensity of the N-CQDs/H_2O_2 system was gradually recovered ("turned on") by the stepwise addition of 100 μL of L-aspartic acid (20 μM) in Fig. 5d. A linear plot was observed for the relative emission. The increase in the PL intensity of the N-CQDs with the addition of L-aspartic acid at an excitation wavelength of 360 nm is shown in Fig. 5e. The obtained limit of detection (LOD) was 134.2 nM, which was calculated by using the equation of $3\sigma/m$ with a linear correlation value of $R^2 = 0.93607$. A comparative analysis of the LOD of N-CQDs for H_2O_2 is shown in Table S2.†

3.4 The fluorescence "on–off–on" mechanism

The exact mechanistic understanding for the fluorescence quenching and restoration of CQDs is not clear. However, some models have been proposed to explain these properties, such as an electronic transition in conjugated sp^2-domains (C=N and C=C) and surface defects of N-CQDs.[54] The PL properties observed in N-CQDs are attributed to the presence of variable surface states including different emissive sites with various oxygenated and nitrogenous functional groups on the N-CQDs surface along with charge carrier recombination.[55,56] When electronegative elements (oxygen and nitrogen) are doped into CQDs, the electrons of higher energy levels of CQDs move towards the more electronegative elements and in consequence, emission intensity is enhanced.[57,58] The increase in PL intensity corresponds to the passivation of nitrogenous and oxygenated groups, such as C–O, COOH, –C=O, =N–H, and –N–H groups. The N-CQDs exhibit a nitrogen and oxygen rich surface, which

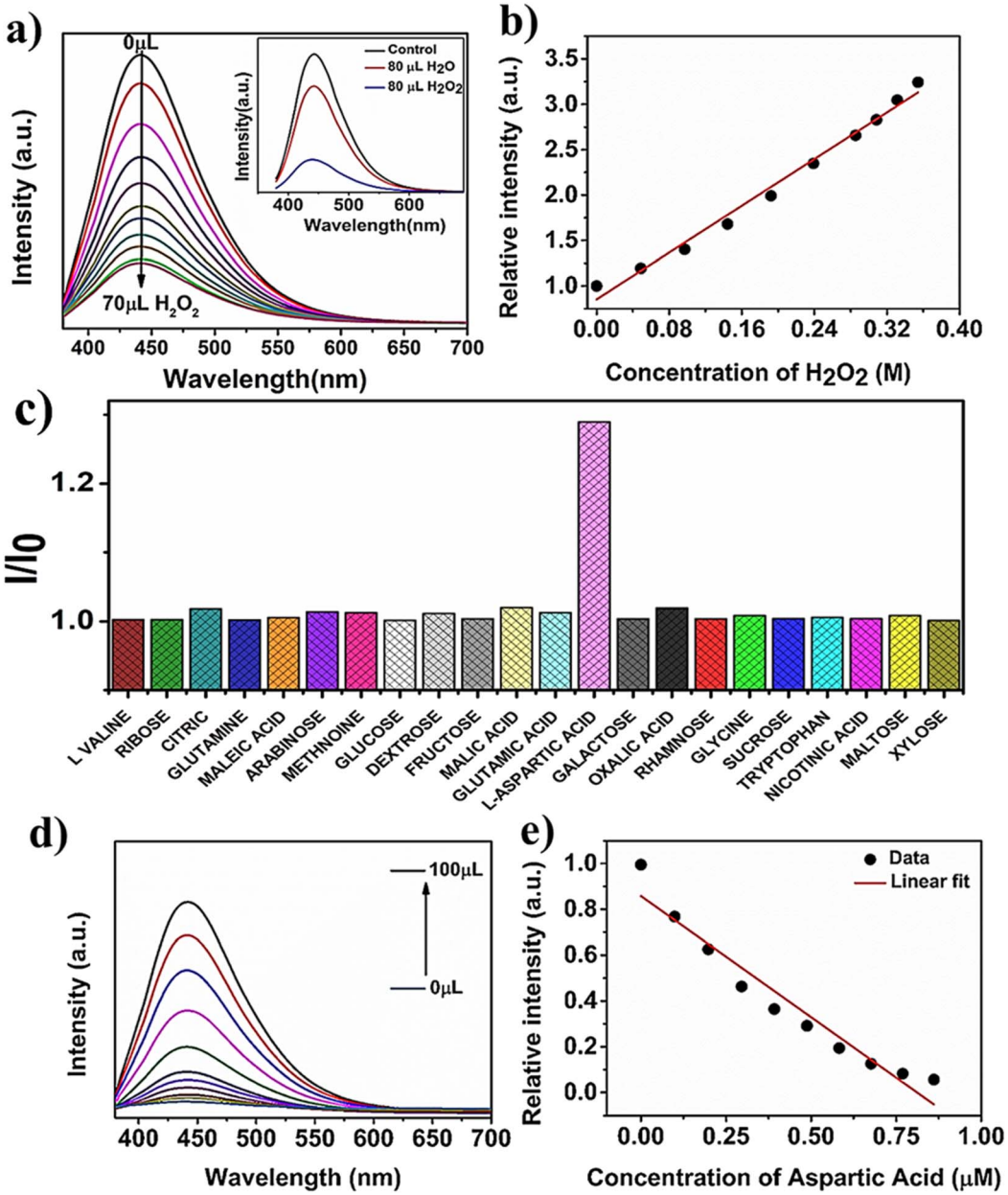

Fig. 5 Sensing applications of N-CQDs towards H_2O_2 and aspartic acid. (a) The effect of water and H_2O_2 on PL emission of N-CQDs. PL intensity varies with the addition of H_2O_2. (b) Linear plot of relative intensity with the concentration of H_2O_2. (c) The addition of biomolecules restored the quenched PL of N-CQDs with high selectivity towards aspartic acid; (d) effect on the PL intensity of N-CQDs/H_2O_2 system with the addition of aspartic acid and (e) linear plot of relative PL intensity with varying concentrations of aspartic acid.

facilitates the transfer of electrons from N-CQDs to H_2O_2 assisted by the FRET mechanism and in consequence results in PL quenching. When H_2O_2 encounters N-CQDs, the electrons from the conduction bands of N-CQDs are transferred to the H_2O_2 *via* the FRET mechanism. The electron transfer by FRET results in a non-radiative recombination of charge carriers and decrease in PL intensity,[59] while the sensitivity towards the H_2O_2 can be explained by the charge transfer mechanism or surface absorption. The stable electrostatic interaction occurring between H_2O_2 and N-CQDs during either charge transfer or change in the states electron density of N-CQDs quenches or "turns off" the PL emission of N-CQDs.[60] Also, abundant surface active sites and functional groups on N-CQDs provide enhanced interaction between N-CQDs and H_2O_2, which favours the FRET based donor–acceptor pair.

When L-aspartic acid was added into such a quenched system a more stable interaction occurred between H_2O_2 and L-aspartic acid because of their strong binding affinity compared to N-CQDs. L-aspartic acid was easily oxidized in the presence of the reactive oxygen species (H_2O_2), thus resulting in restoration or "turning on" of the PL intensity of N-CQDs.[61] The FRET process is inhibited because of the cleavage of FRET pairs and

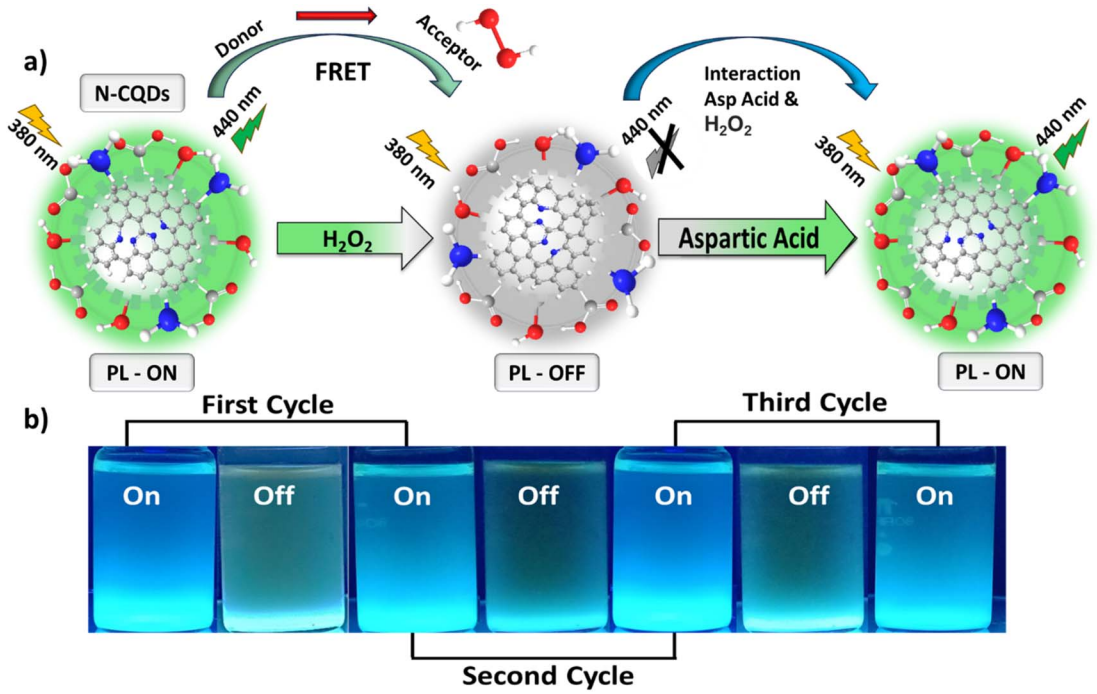

Fig. 6 The fluorescence "on–off–on" mechanism (a) and (b) cycling stability of N-CQDs.

the N-CQDs are free, which resulted in an enhancement in quenched PL intensity or "turn on". This "turn on" PL intensity shows good linearity with the increase in concentration of L-aspartic acid. A comparison of the N-CQDs based optical probes for the detection of H_2O_2 and L-aspartic acid with other probes is shown in Table S1 and S2,† respectively. The applicability and high reversibility of the as-synthesized N-CQDs for fluorescence-based nano-switching ("on–off–on") exhibits significant potential for practical applications in biomarker and biomolecular detection. Fig. 6a shows the schematic representation of the PL "on–off–on" mechanism for the selective and sensitive sensing of H_2O_2 and aspartic acid. Fig. 6b shows the visual images of the cycling stability of N-CQDs for the three cycles of PL "on–off–on" based detection of H_2O_2 and aspartic acid. These results suggested that as-synthesized N-CQDs are an efficient fluorescence-based material for the selective sensing of H_2O_2 and L-aspartic acid with a fluorescence "on–off–on" mechanism.

4. Conclusion

N-doped CQDs were synthesized by taking drumstick leaves as precursors *via* a simple hydrothermal process. The N-CQDs with a uniform morphology and particle size exhibit good photostability, aqueous solubility and FRET process. Based upon FRET a PL "on–off–on" platform has been developed for the detection of H_2O_2 and aspartic acid with good selectivity and high sensitivity. The PL intensity of N-CQDs was "turned off" (quenched) in the presence of H_2O_2, with a LOD 26.4 mM. The PL intensity of the quenched system of N-CQDs-H_2O_2 was selectively regained or "turned on" with a good linear response by the addition of L-aspartic acid. Furthermore, these N-CQDs based biosensors exhibit good reversibility and high stability, which can be extended for practical diagnostic applications.

Conflicts of interest

No competitive or financial interest.

Acknowledgements

KMT acknowledges financial assistance from the Department of Biotechnology (DBT), India, through the Ramalingaswami Faculty Award (BT/RLF/Re-entry/45/2018). KSR thanks the DBT for financial support. GSD thanks IIPE for fellowship.

References

1 G. Allison, A. K. Sana, Y. Ogawa, H. Kato, K. Ueno, H. Misawa, K. Hayashi and H. Suzuki, *Nat. Commun.*, 2021, **12**, 6483.
2 O. Pashchenko, T. Shelby, T. Banerjee and S. Santra, *ACS Infect. Dis.*, 2018, **4**, 1162–1178.
3 N. Liu, Z. Xu, A. Morrin and X. Luo, *Anal. Methods*, 2019, **11**, 702–711.
4 A. G. Brolo, *Nat. Photonics*, 2012, **6**, 709–713.
5 F. S. Ligler and J. J. Gooding, *Anal. Chem.*, 2019, **91**, 8732–8738.
6 K. M. Tripathi, T. Kim, D. Losic and T. T. Tung, *Carbon*, 2016, **110**, 97–129.
7 A. Sharma, N. Sharma, A. Kumari, H.-J. Lee, T. Kim and K. M. Tripathi, *Appl. Mater. Today*, 2020, **18**, 100467.

8 J. Lu, H. Zhang, S. Li, S. Guo, L. Shen, T. Zhou, H. Zhong, L. Wu, Q. Meng and Y. Zhang, *Inorg. Chem.*, 2020, **59**, 3152–3159.
9 V. Muhr, M. Buchner, T. Hirsch, D. J. Jovanović, S. D. Dolić, M. D. Dramićanin and O. S. Wolfbeis, *Sens. Actuators, B*, 2017, **241**, 349–356.
10 F. Johnson and C. Giulivi, *Mol. Aspects Med.*, 2005, **26**, 340–352.
11 M. Giorgio, M. Trinei, E. Migliaccio and P. G. Pelicci, *Nat. Rev. Mol. Cell Biol.*, 2007, **8**, 722–728.
12 C. Lennicke, J. Rahn, R. Lichtenfels, L. A. Wessjohann and B. Seliger, *Cell Commun. Signaling*, 2015, **13**, 39.
13 B. Halliwell, M. V. Clement and L. H. Long, *FEBS Lett.*, 2000, **486**, 10–13.
14 R. A. Stolarek, P. Białasiewicz, M. Król and D. Nowak, *Clin. Chim. Acta*, 2010, **411**(23–24), 1849–1861.
15 C. Yu, L. Wang, W. Li, C. Zhu, N. Bao and H. Gu, *Sens. Actuators, B*, 2015, **211**, 17–24.
16 Y. Izumi, I. Chibata and T. Itoh, *Angew. Chem., Int. Ed. Engl.*, 1978, **17**, 176–183.
17 P. Chauhan, J. Saini, S. Chaudhary and K. K. Bhasin, *Mater. Res. Bull.*, 2021, **134**, 111113.
18 B. B. Prasad and I. Pandey, *Electrochim. Acta*, 2013, **88**, 24–34.
19 M. M. Alam, A. M. Asiri, M. A. Hasnat and M. M. Rahman, *Biosensors*, 2022, **12**, 379.
20 A.-F. Yang, S.-L. Hou, Y. Shi, G.-L. Yang, D.-B. Qin and B. Zhao, *Inorg. Chem.*, 2019, **58**, 6356–6362.
21 M. H. Baslow and T. R. Resnik, *J. Mol. Neurosci.*, 1997, **9**, 109–125.
22 J. Gao, D. Lv, H. Sun and W. Yang, *J. Braz. Chem. Soc.*, 2009, **20**, 1827–1832.
23 C. Ji, Y. Zhou, R. M. Leblanc and Z. Peng, *ACS Sens.*, 2020, **5**, 2724–2741.
24 H. Dong, W. Gao, F. Yan, H. Ji and H. Ju, *Anal. Chem.*, 2010, **82**, 5511–5517.
25 D. Wu, A. C. Sedgwick, T. Gunnlaugsson, E. U. Akkaya, J. Yoon and T. D. James, *Chem. Soc. Rev.*, 2017, **46**, 7105–7123.
26 X. Xie, W. Zhang, A. Abbaspourrad, J. Ahn, A. Bader, S. Bose, A. Vegas, J. Lin, J. Tao, T. Hang, H. Lee, N. Iverson, G. Bisker, L. Li, M. S. Strano, D. A. Weitz and D. G. Anderson, *Nano Lett.*, 2017, **17**, 2015–2020.
27 Z. Wang, D. Chen, B. Gu, B. Gao, T. Wang, Q. Guo and G. Wang, *Spectrochim. Acta, Part A*, 2020, **227**, 117671.
28 D. Song, J. Tian, W. Xu, H. Wen, C. Wang, J. Tang, J. Zhang and M. Guo, *Carbon*, 2021, **174**, 741–749.
29 L. Cao, X. Wang, M. J. Meziani, F. Lu, H. Wang, P. G. Luo, Y. Lin, B. A. Harruff, L. M. Veca, D. Murray, S.-Y. Xie and Y.-P. Sun, *J. Am. Chem. Soc.*, 2007, **129**, 11318–11319.
30 D. R. Larson, W. R. Zipfel, R. M. Williams, S. W. Clark, M. P. Bruchez, F. W. Wise and W. W. Webb, *Science*, 2003, **300**, 1434–1436.
31 M. Pourmadadi, E. Rahmani, M. Rajabzadeh-Khosroshahi, A. Samadi, R. Behzadmehr, A. Rahdar and L. F. R. Ferreira, *J. Drug Delivery Sci. Technol.*, 2023, **80**, 104156.
32 A. H. Loo, Z. Sofer, D. Bouša, P. Ulbrich, A. Bonanni and M. Pumera, *ACS Appl. Mater. Interfaces*, 2016, **8**, 1951–1957.
33 A. Sharma, R. K. Sharma, Y.-K. Kim, H.-J. Lee and K. M. Tripathi, *J. Environ. Chem. Eng.*, 2021, **9**, 106656.
34 D. Saini, Gunture, J. Kaushik, R. Aggarwal, K. M. Tripathi and S. K. Sonkar, *ACS Appl. Nano Mater.*, 2021, **4**, 12825–12844.
35 C. a. Ma, C. Yin, Y. Fan, X. Yang and X. Zhou, *J. Mater. Sci.*, 2019, **54**, 9372–9384.
36 H. Kalita, V. S. Palaparthy, M. S. Baghini and M. Aslam, *Carbon*, 2020, **165**, 9–17.
37 T. V. de Medeiros, J. Manioudakis, F. Noun, J.-R. Macairan, F. Victoria and R. Naccache, *J. Mater. Chem. C*, 2019, **7**, 7175–7195.
38 X. Feng and Y. Zhang, *RSC Adv.*, 2019, **9**, 33789–33793.
39 G. Hu, L. Ge, Y. Li, M. Mukhtar, B. Shen, D. Yang and J. Li, *J. Colloid Interface Sci.*, 2020, **579**, 96–108.
40 C. Hu, Y. Liu, Y. Yang, J. Cui, Z. Huang, Y. Wang, L. Yang, H. Wang, Y. Xiao and J. Rong, *J. Mater. Chem. B*, 2013, **1**, 39–42.
41 S. K. Park, H. Lee, M. S. Choi, D. H. Suh, P. Nakhanivej and H. S. Park, *Energy Stor. Mater.*, 2018, **12**, 331–340.
42 G. Yang, C. Wu, X. Luo, X. Liu, Y. Gao, P. Wu, C. Cai and S. S. Saavedra, *J. Phys. Chem. C*, 2018, **122**, 6483–6492.
43 Z. Wang, J. Yu, X. Zhang, N. Li, B. Liu, Y. Li, Y. Wang, W. Wang, Y. Li, L. Zhang, S. Dissanayake, S. L. Suib and L. Sun, *ACS Appl. Mater. Interfaces*, 2016, **8**, 1434–1439.
44 G. S. Das, A. Bhatnagar, P. Yli-Pirilä, K. M. Tripathi and T. Kim, *Chem. Commun.*, 2020, **56**, 6953–6956.
45 G. S. Das, J. P. Shim, A. Bhatnagar, K. M. Tripathi and T. Kim, *Sci. Rep.*, 2019, **9**, 15084.
46 S. Jung, Y. Myung, G. S. Das, A. Bhatnagar, J.-W. Park, K. M. Tripathi and T. Kim, *New J. Chem.*, 2020, **44**, 7369–7375.
47 J. Kaushik, C. Sharma, N. K. Lamba, P. Sharma, G. S. Das, K. M. Tripathi, R. K. Joshi and S. K. Sonkar, *Langmuir*, 2023, **39**, 12865–12877.
48 G. S. Das, K. M. Tripathi, G. Kumar, S. Paul, S. Mehara, S. Bhowmik, B. Pakhira, S. Sarkar, M. Roy and T. Kim, *New J. Chem.*, 2019, **43**, 14575–14583.
49 R. Atchudan, T. N. J. I. Edison, S. Perumal, N. Muthuchamy and Y. R. Lee, *J. Photochem. Photobiol., A*, 2020, **390**, 112336.
50 G. S. Das, J. Y. Hwang, J.-H. Jang, K. M. Tripathi and T. Kim, *ACS Appl. Energy Mater.*, 2022, **5**, 6663–6670.
51 P. Krishnaiah, R. Atchudan, S. Perumal, E.-S. Salama, Y. R. Lee and B.-H. Jeon, *Chemosphere*, 2022, **286**, 131764.
52 N. Thongsai, P. Jaiyong, S. Kladsomboon, I. In and P. Paoprasert, *Appl. Surf. Sci.*, 2019, **487**, 1233–1244.
53 V. K. Tripathi, G. S. Das, R. K. Gupta, M. Srivastava and K. M. Tripathi, *RSC Sustainability*, 2023, **1**, 2319–2327.
54 Q. Ye, F. Yan, Y. Luo, Y. Wang, X. Zhou and L. Chen, *Spectrochim. Acta, Part A*, 2017, **173**, 854–862.
55 A. K. Garg, C. Dalal, J. Kaushik, S. R. Anand and S. K. Sonkar, *Mater. Today Sustain.*, 2022, **20**, 100202.
56 R. Aggarwal, A. K. Garg, V. Kumar, H. Jonwal, S. Sethi, S. Gadiyaram, S. K. Sonkar, A. K. Sonker and G. Westman, *ACS Appl. Nano Mater.*, 2023, **6**, 6518–6527.

57 X. Wang, L. Cao, F. Lu, M. J. Meziani, H. Li, G. Qi, B. Zhou, B. A. Harruff, F. Kermarrec and Y.-P. Sun, *Chem. Commun.*, 2009, 3774–3776.
58 H. Qi, Z. Zhai, X. Dong and P. Zhang, *Spectrochim. Acta, Part A*, 2022, **279**, 121456.
59 K. Phukan, R. R. Sarma, S. Dash, R. Devi and D. Chowdhury, *Nanoscale Adv.*, 2022, **4**, 138–149.
60 Y. Yi, J. Deng, Y. Zhang, H. Li and S. Yao, *Chem. Commun.*, 2013, **49**, 612–614.
61 B. Ticconi, A. Colcerasa, S. Di Stefano, O. Lanzalunga, A. Lapi, M. Mazzonna and G. Olivo, *RSC Adv.*, 2018, **8**, 19144–19151.